PCCP

RSC Publishing

PAPER

A comparative study of electronic properties of disordered conjugated polymers†

Cite this: *Phys. Chem. Chem. Phys.*, 2013, **15**, 3543

Nenad Vukmirović*

Received 5th September 2012,
Accepted 9th January 2013

DOI: 10.1039/c3cp43115k

www.rsc.org/pccp

The comparison of hole density of states (DOS) and hole mobilities of several organic polymer based systems was performed to gain insight into the main factors that determine the electrical properties of conjugated polymers. The DOS and the mobility of the systems under investigation were evaluated using an atomistic multiscale procedure. The results suggest that the irregularities in the shape of the polymer chains increase the diagonal disorder, while alkyl side chains act as spacers that reduce the diagonal disorder which originates from long range electrostatic interactions. Intrachain electronic coupling in relatively ordered polymers narrows the tail of the DOS, while in less ordered polymers it represents the additional component of disorder and widens the tail of the DOS. The width of the DOS tail was confirmed to be an important factor that determines the activation energy for charge carrier transport. However, it is not the only factor since the system with a smaller width of the DOS tail can have a larger activation energy due to, for example, smaller wave function overlap between transport states.

1 Introduction

There is great interest to understand the electronic properties of semiconducting conjugated polymers – the constituent materials of organic electronic devices.[1–11] This is a significant challenge due to the complex structure of these materials. Depending on the processing conditions, polymer chains are arranged either in an amorphous spaghetti-like structure or form ordered domains with amorphous regions at their boundaries.[12,13] In each of these cases, there is a certain degree of disorder which has a strong influence on the electronic properties of the material and consequently on the operation of organic electronic devices. The fingerprint of the presence of disorder in the electronic spectrum is the tail in the DOS at the conduction and valence band edges. The width of this tail increases as the disorder increases. Understanding the factors that determine the strength of the disorder is of utmost importance for possible future designs of organic electronic devices.

A widely used procedure for modelling the effects of disorder in these materials is to assume a certain form of the electronic DOS (typically a Gaussian[14–16] or an exponential[17] function), a certain spatial distribution of these states (typically a square lattice or a uniform random distribution) and a certain form of transition rates between the states.[14–17] The parameters of such models are then extracted from fits to experimental mobility measurements. However, such a procedure can only be used for an *a posteriori* analysis of the experimental data. It does not have the predictive power and consequently cannot be used in the design of new materials and the search for better materials.

On the other hand, the calculations performed on straight polymer chains or on monomers are often practised.[18–22] Such calculations can certainly be insightful when an estimate of the band gap and the absorption spectrum of the polymer is concerned. However, they give no information on the degree of disorder in realistic materials simply because these are performed on a system with no disorder.

In recent years, approaches have been developed to calculate the electronic DOS and electronic transport properties of disordered polymer-based materials starting from the chemical formula of the polymer.[23–31] Such approaches are therefore free of any phenomenological parameters. In these approaches one typically obtains the atomic structure of the material from classical molecular dynamics simulations. The obtained atomic structure is then used as input for electronic structure calculations. If electronic transport properties are desired, hopping probabilities between electronic states can be also obtained and the electrical transport properties can be extracted from a master equation or the kinetic Monte Carlo approach. Therefore, these approaches in principle establish the relationship between the structure of the material and its electrical

Scientific Computing Laboratory, Institute of Physics Belgrade, University of Belgrade, Pregrevica 118, 11080 Belgrade, Serbia.
E-mail: nenad.vukmirovic@ipb.ac.rs

† Electronic supplementary information (ESI) available: Six supplementary figures. See DOI: 10.1039/c3cp43115k

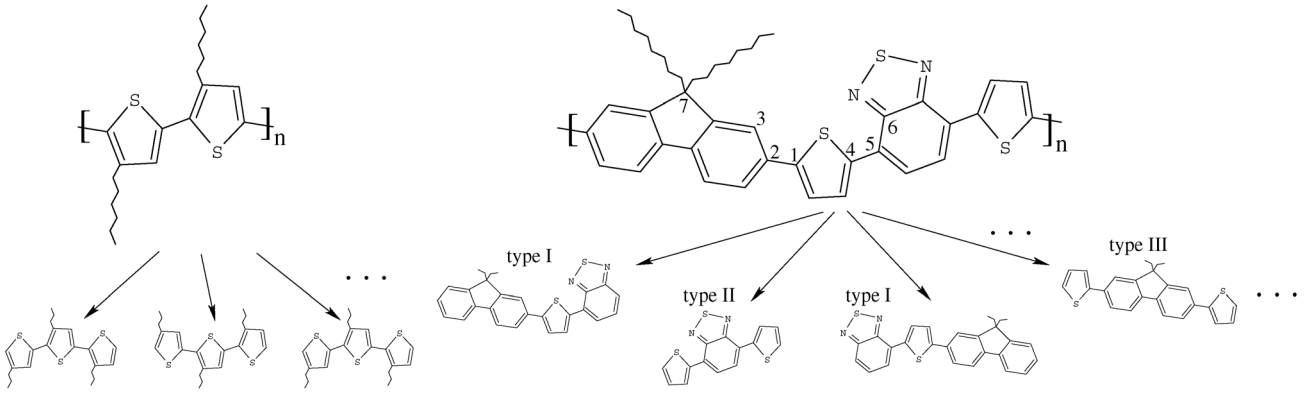

Fig. 1 Structural formula of the P3HT (top left) and the APFO3 polymer (top right). Schemes for the division of the polymers into fragments in OFM calculations (bottom).

properties and can be potentially used to design materials with better electrical transport characteristics.

However, at present we are still not able to use such approaches to routinely design new materials for several reasons. There is a lack of force-field parameters for molecular dynamics simulations and one needs to adjust the force field to calculate a new material.[24] Large supercells and a large number of repeated calculations are required to get enough statistics for accurate DOS from electronic structure calculations.[27,30] Furthermore, one typically needs to use specialized methods for electronic structure calculations which are not yet practised among a wide pool of researchers.[27,32,33] Finally, these calculation procedures are computationally rather demanding and consequently they are typically performed for a single material only. For these reasons, a systematic search over a certain space of envisaged materials is hindered by both the computational and human burden involved.

At the present stage of development, one can (and arguably should) therefore take a different route to benefit most from the capability to perform large-scale electronic structure and electronic transport calculations of disordered conjugated polymers. These simulations can be used to understand the main factors that determine the width of the tail of the DOS, as well as the transport properties. In particular, some of the questions that may be posed are the following. What is the role of alkyl side chains and does their presence necessarily reduce the carrier mobility? How does the shape of the main chain affect the electronic properties? What is the effect of the chemical structure of the monomer? What is the difference in the properties of the material based on monomers and polymers? With answers to such questions at hand, one will be in a position to devise several rules of thumb that should lead the development of new materials that exhibit better device characteristics.

In this work, a comparative study of electronic properties of poly(3-hexylthiophene) (P3HT) polymer, a polyfluorene copolymer poly[2,7-(9,9-dioctyl-fluorene)-alt-5,5-(4′,7′-di-2-thienyl-2′,1′,3-benzothiadiazole)] (APFO3) and APFO3 in its monomer form with and without alkyl side chains is performed. P3HT is possibly the most studied conjugated polymer,[34–38] while the APFO3 polymer has also recently been widely investigated.[39–46] Structural formulae of P3HT and APFO3 polymers are presented in Fig. 1. The choice of systems for this study was made to enable significant insight into the answers to many of the questions posed above. The electronic DOS and the DC mobility of these systems were evaluated using recently introduced methods for large-scale electronic structure and electronic transport calculations.

On the basis of the simulation results, it was found that the alkyl chains act, on the one hand, as spacers that reduce the electrostatic disorder introduced by the presence of other main chains and, on the other hand, as insulating barriers that impede the charge carrier transport. Their overall effect on charge carrier mobility depends on the interplay of these two effects. The results also indicate that irregularities in the shape of the main chains increase the electrostatic disorder in the material. It is shown next that monomer and polymer based materials have a similar degree of diagonal disorder. However, the polymer material has a better mobility due to the presence of intrachain electronic coupling. The chemical structure of the material determines all the mentioned properties mainly through: (1) the interring torsion potential that determines the shape of the main chains; (2) the atomic charges that define the strength of electrostatic disorder.

2 Computational methodology

The computational methodology used to obtain the electronic DOS and the DC mobility is based on a multiscale procedure introduced in ref. 47 and 48. The main steps of the procedure are briefly outlined here.

Atomic structure of the amorphous polymer material is obtained from classical molecular dynamics using a simulated annealing procedure. Polymer chains are initially placed in a volume much larger than that corresponding to the density of the material and a high temperature of $T = 1000$ K is imposed. The volume of the system is then slowly decreased down to that corresponding to the experimental density of the material which is 1 g cm^{-3} for the APFO3 polymer and monomer with side chains,[49] and 1.1 g cm^{-3} for the P3HT polymer.[50–53] It was also checked in the simulation that minimal energy of the system is achieved at these densities. The density of the APFO3 monomer without side chains (where experimental data were

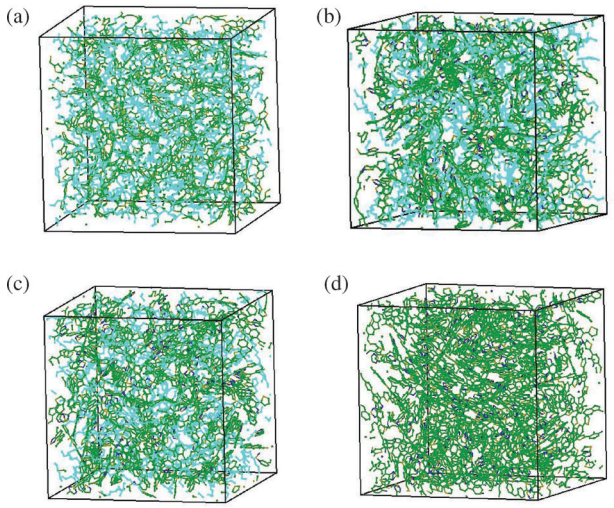

Fig. 2 Atomic structures obtained using a simulated annealing procedure for: (a) P3HT (12 024 atoms divided into 12 chains with 40 units); (b) APFO3 polymer (11 304 atoms divided into 12 chains with 10 units); (c) APFO3 monomer with side chains (11 520 atoms consisting of 120 monomers); (d) APFO3 monomer without side chains (11 400 atoms consisting of 190 monomers). C atoms of the main chain are shown in green, N atoms in dark blue, S atoms in dark yellow, C atoms of the alkyl side chains in light blue, while H atoms are not shown.

not available) was found from the simulation to be equal to 1.28 g cm^{-3}. Finally, the system was gradually cooled down to room temperature and relaxed to a local minimum. The classical CFF91 force field[54,55] was used to describe the interatomic interaction. Since classical force fields typically do not properly describe the interring torsion profiles of polymers, these profiles were calculated from quantum chemical calculations and the force field was modified to properly reproduce the torsion profiles. One realization of the atomic structure for each of the systems studied is shown in Fig. 2.

Electronic structure was obtained using the charge patching method (CPM)[32] and the overlapping fragments method (OFM).[30,33]

CPM is a method for the construction of a single-particle Hamiltonian with the accuracy similar to that of density functional theory (DFT) in local density approximation (LDA). It is based on the idea that the charge density in the neighbourhood of an atom depends only on the local atomic environment. By exploiting this idea, one constructs the charge density of a large system by adding the contributions of each atom in the system – so-called motifs. The motifs are extracted from a full DFT/LDA calculation of a small prototype system where atoms have the same bonding environment as in the large system that one wants to calculate. From the charge density, one constructs the single-particle potential by solving the Poisson equation for the Hartree potential and using the LDA formula for the exchange–correlation potential. The CPM was used with success in the past in the studies of a variety of semiconducting materials and nanostructures, such as carbon fullerenes,[56] semiconductor alloys,[57] impurities in semiconductors,[58] organic molecules and polymers,[32] and semiconductor quantum dots.[59] The accuracy of the CPM in the case of the P3HT polymer was verified in ref. 29, while the test that demonstrates its accuracy in the case of APFO3 is reported in Fig. S1 in ESI.† On the basis of previous applications and validations of CPM, one can say that it performs quite well for a wide range of semiconducting systems where there is no long range charge transfer.

OFM is a method for the diagonalisation of the single particle Hamiltonian obtained, for example, using the CPM. The system is divided into fragments that are mutually overlapping and the Hamiltonian is represented on the basis of molecular orbitals of these fragments. Wave functions of fragment orbitals were represented using the basis of plane waves with a kinetic energy cut-off of 60 Ry. The scheme for the division of the polymers studied in this work into fragments is given in Fig. 1. For accurate representation of the eigenstates at the top of the valence band, it is sufficient to include only a few highest occupied molecular orbitals of the fragment; for materials studied in this work only one orbital per fragment was sufficient. Consequently, the main advantage of this method is that the size of the basis is quite small. The use of CPM and OFM enables the calculation of relevant electronic states with the accuracy similar to that in DFT/LDA but with a much smaller computational cost. The accuracy of the OFM for the P3HT polymer was demonstrated in ref. 33, while the test of its performance in the case of the APFO3 polymer is given in Fig. S2 in ESI.† One should note that the proper choice of fragments is essential for the accuracy of this method and therefore similar tests are always performed before the main calculations are done.

In disordered materials, charge carrier wave functions of band edge states are localised to small regions of space. As a consequence, electrical transport can take place only by carrier hopping between localised states. In this work, it is assumed that charge carriers are holes and that this hopping takes place due to electron–phonon interaction that acts as a perturbation. Another possible source of localisation in organic materials (in particular small molecule based crystalline semiconductors) is small polaron formation, which is present if electron–phonon interaction is sufficiently large. DFT calculations[60,61] based either on LDA[60] or B3LYP[61] functionals have shown that polaron binding energy in long straight polythiophene chains is of the order of few meVs only. Therefore, it has been argued in ref. 60 and 62 that polaron effects could be ignored in practice. It still remains unclear whether a conclusion based on calculations on ordered polymer chains can be extended to disordered polymers. Our calculations (reported in Section 5 in ESI of ref. 47) indicated that this is largely the case. Therefore, it is assumed in this work that the main source of wave function localisation is the disorder and that carrier binding to the lattice (polaron formation) may lead only to some additional localisation (possibly followed by the increase in activation energy) whose effect is neglected. It would nevertheless be very interesting to develop a theory which would take into account both the effects of disorder and polaron formation on equal footing but that seems to be a tremendously difficult task at present.

The transition rate W_{ij} for downhill hop between electronic states i and j is calculated as

$$W_{ij} = \beta^2 \mathscr{S}_{ij}{}^2 [N(\varepsilon_{ij}) + 1] D_{\mathrm{ph}}(\varepsilon_{ij})/\varepsilon_{ij}, \qquad (1)$$

where $\mathscr{S}_{ij} = \int d^3\boldsymbol{r}|\psi_i(\boldsymbol{r})| \cdot |\psi_j(\boldsymbol{r})|$ is the overlap of the wave function moduli, $D_{\mathrm{ph}}(E)$ is the phonon DOS normalized to satisfy $\int_0^\infty D_{\mathrm{ph}}(E)dE = 1$, $N(E) = \left(\exp\frac{E}{k_B T} - 1\right)^{-1}$ is the phonon occupation number given by the Bose–Einstein distribution at a temperature T, $\varepsilon_{ij} = |\varepsilon_i - \varepsilon_j|$ with ε_i being the energy of electronic state i. Eqn (1) is a good approximation to the expression that is obtained if one takes into account the details of the interaction of electrons with all phonon modes.[63] In eqn (1), the factor β is the proportionality factor between the electron–phonon coupling element and the wave function moduli overlap. It is equal to 10^7 eV $s^{-1/2}$ for P3HT[63] and 3.7×10^6 eV $s^{-1/2}$ for the APFO3 polymer (the latter value was obtained using the same procedure as in ref. 63 in the case of P3HT). It was shown in the past that the DC mobility calculated using eqn (1) gives practically the same result (within a few percent) as if a more detailed formula were used.[63]

The calculations of electronic states and the transition rates between these states are performed for the system of the size $\sim$5 nm. Such box dimensions are significantly larger than the wave function localisation lengths (see Fig. S3 in ESI†) and therefore finite size effects do not affect the calculation of transition rates. However, these dimensions are not sufficiently large to obtain the mobility which is independent of the realization of the system. Therefore, a multiscale procedure is adopted where the calculation of electronic structure is repeated many ($\sim$50) times and a larger $10 \times 10 \times 10$ system is constructed. Each cell in the $10 \times 10 \times 10$ system corresponds to one calculation on the previous length scale. It turns out that the fluctuations in the mobility for different realizations of the system are present even for the system of this size and one needs to go one length scale further. At the final length scale, a new $10 \times 10 \times 10$ system is constructed where each cell is a homogeneous anisotropic conductor whose conductivity is obtained from the simulation on the previous length scale. The reader is referred to ref. 47 and 48 for details of the implementation of the multiscale procedure and seamless transition between different length scales.

The described approach evaluates the mobility using the microscopic information about the material and does not introduce any assumptions about the spatial and energetic distribution of states and the transition rates, unlike most of the phenomenological models in the literature. Nevertheless, it is interesting to understand which of the simple and insightful models from the literature has similar features to the results of our approach. We have shown in the past[47] that hopping over a range of distances is relevant, in line with the picture of the variable-range hopping model[62] (and in contrast to nearest neighbour hopping). In addition, we found[30] that the mobility-edge model is not appropriate, as the analysis of the dependence of wave function localisation lengths on energies did not indicate any apparent mobility edge energy in the sense that wave function localisation–delocalisation transition takes place at that energy.

3 Results and discussion

The main strength of the computational approach used in this work is its ability to fully take into account the effects of disorder. On the macroscopic level, the effects of disorder are manifested *via* the tail of the DOS near the band edge and *via* thermally activated carrier mobility. The simulations allow us to investigate the microscopic origin of the effects of disorder and in turn understand the differences in disorder of various materials. It should be pointed out that the same material can exhibit various characteristics depending on the processing conditions which strongly affect the morphology of the material. Nevertheless, the comparison of different materials performed in this work is fair because the same procedure was used to generate the atomic structure of the material in all cases.

3.1 Diagonal disorder

To quantify the effects of disorder on the microscopic scale, the onsite Hamiltonian matrix elements $\langle i|H|i\rangle$ are evaluated, where i is the highest occupied molecular orbital of a fragment and H the single-particle Hamiltonian. In a straight polymer this matrix element would be the same for all fragments of the same type. Spatial fluctuations of this matrix element (these fluctuations will be called ''diagonal disorder'' in what follows) therefore give a microscopic quantification of the effects of disorder.

In Fig. 3, the distribution of onsite Hamiltonian matrix elements is presented for all systems studied in this work. One should note that all fragments in P3HT have the same structural formula, while in the case of APFO3 there are several types of fragments. Therefore, to have a fair comparison between P3HT and APFO3 based materials, only the matrix elements corresponding to the fragments of the same type (type II, see Fig. 1) are considered in the case of APFO3-based materials.

Two groups of factors lead to spatial fluctuations of onsite Hamiltonian matrix elements – the fluctuations in the shape of the fragment and the fluctuations caused by the environment of the fragment. The fluctuations caused by the environment originate from the long range electrostatic potential created by the charges in the rest of the system. Such fluctuations are prominent if there is a certain type of short range charge transfer in the system, either within the ring in the case of P3HT or between the donor and acceptor part in the case of APFO3. In such cases, the environment can be considered as a set of dipoles with various orientations whose potential causes the fluctuations of onsite Hamiltonian matrix elements. The dipoles typically originate from the main polymer chain, since there is very little charge transfer in alkyl side chains. The degree of these fluctuations will depend on the degree of randomness of dipole orientations, the strength of the dipoles and their distances from the fragment under consideration.

The comparison of the distribution of onsite elements in P3HT and APFO3 polymers (Fig. 3, top left and bottom left) implies that the diagonal disorder is stronger in P3HT than in APFO3. Possible origins of this difference have been discussed in the previous paragraph. To narrow down the choice between these possibilities, further analysis is performed as follows. Two effects discussed in the previous section are closely related to the shape of the main chains: the fluctuations in the shape of the fragment and the degree of randomness of dipole orientations. The shape of the main chains is entirely determined by

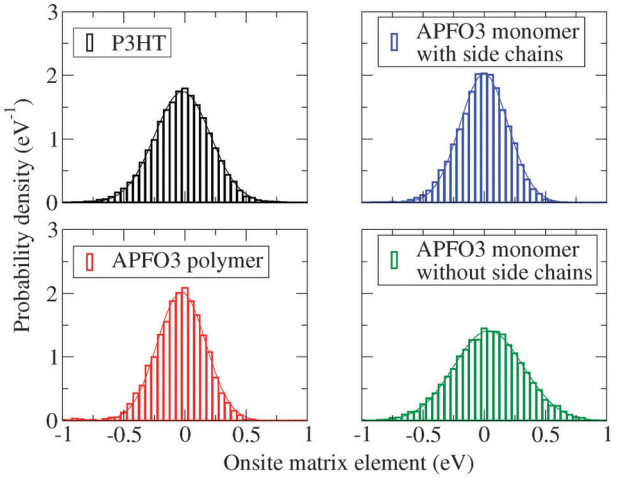

Fig. 3 Distribution of the values of onsite Hamiltonian matrix elements. The lines represent the fits of histograms to a Gaussian distribution – the best fit is obtained at σ = 228 meV (P3HT), σ = 197 meV (APFO3 polymer), σ = 197 meV (APFO3 monomer with side chains) and σ = 282 meV (APFO3 monomer without side chains). In the case of APFO3-based materials, the distribution includes type II fragments only.

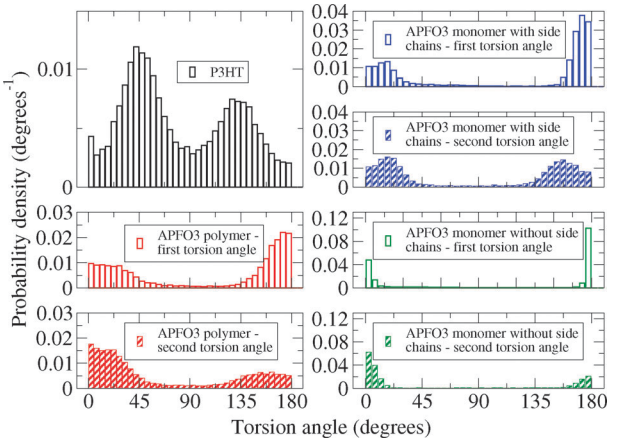

Fig. 4 Distribution of interring torsion angles in the systems under study. In APFO3 polymers, there are two types of interring torsion angles: first torsion angle refers to the angle S456 in Fig. 1, while second torsion angle refers to the angle S123 in Fig. 1.

the interring torsion angles. For this reason, the distribution of interring torsion angles for materials studied in this work is presented in Fig. 4. In P3HT, practically all torsion angles are allowed and the chain has a highly disordered shape. On the other hand, in the APFO3 polymer, the torsion angles near 0° and 180° are favoured and the main chain has a relatively ordered shape. As a consequence, a more disordered shape of P3HT causes stronger diagonal disorder in P3HT compared to that in APFO3. When the remaining effects are concerned, one should not expect that the distances of dipoles from the fragment under consideration should be overall different in one system or the other. Both systems have alkyl side chains of similar length attached to the main chain. These alkyl chains fill the space between the main chains and given their similar length, one may expect that the distances between fragments of different main chains are overall similar in both systems. Finally, when the strength of the dipoles is concerned, there are no strong differences between P3HT and APFO3 for the following reasons. Charge transfer within the thiophene ring in APFO3 is overall similar to the charge transfer within the thiophene ring in P3HT – for example the S atom charge in the thiophene ring in APFO3 is 0.13, while it is equal to 0.16 in P3HT. The amount of charge transfer between different units in APFO3 is also relatively small – the charge distribution in APFO3 is composed of a transfer of 0.04 electrons from the thiophene ring to the benzothiadiazole part and of a transfer of 0.01 electrons from the fluorene part to the thiophene ring. For these reasons, it is not expected that the differences in dipole strengths of the two systems can be the principal reason for differences of diagonal disorder in two materials.

However, it appears to be not straightforward to identify the contributions of all mentioned effects from a comparison of two different polymer systems. Therefore, to further clearly illustrate the mentioned effects, comparisons of very similar systems were made: between the APFO3 polymer and the APFO3 monomer, as well as between APFO3 monomers with and without side chains.

The APFO3 polymer and the APFO3 monomer have a very similar distribution of interring torsion angles, the same strength of the dipoles and very similar distribution of distances between fragments of different chains. As a consequence, one should expect nearly the same distribution of onsite matrix elements. Indeed, as seen from Fig. 3 (bottom left and top right), this distribution is nearly the same.

Materials based on the APFO3 monomer with and without side chains have pronouncedly different distances of dipoles from fragments (see Fig. S4 in ESI†) and one therefore expects a wider distribution of onsite elements in the case of the APFO3 monomer without side chains. In line with such expectations one finds a much wider distribution of onsite elements in the APFO3 monomer without side chains. One should also note that there is a certain degree of ordering that takes place in the APFO3 monomer without side chains. The interring torsion angles (Fig. 4) have a very narrow distribution at angles very close to 0° and 180° in contrast to the APFO3 monomer with side chains which has a somewhat wider distribution centred around the same angles. In addition, the distribution of the cosine of the angle between the planes of two nearest neighbour monomers is shown in Fig. 5. In the APFO3 monomer with side chains this distribution is nearly uniform, as in a system with fully randomly oriented molecules. On the other hand, in the APFO3 monomer without side chains this distribution clearly differs from a uniform one, which is another signature of a certain degree of ordering. To summarize this comparison, some ordering takes place in the APFO3 monomer without side chains. Nevertheless, the fact that it has a much wider distribution of onsite Hamiltonian matrix elements indicates that the effect of proximity of the dipoles from the fragment is much stronger than the effect of ordering. Such a conclusion is rather expected since the onsite disorder in the system of closely spaced dipoles can be weaker than in the case

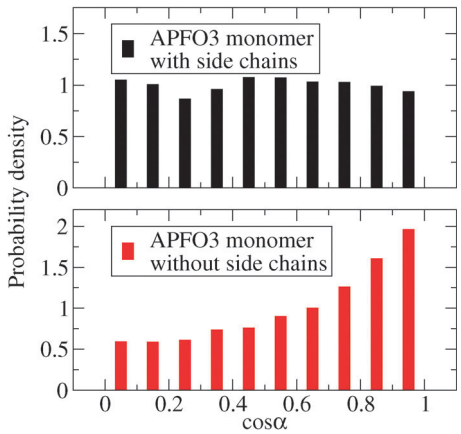

Fig. 5 Distribution of $\cos\alpha$, where α is the angle between the planes of two nearest neighbour monomers in the materials based on APFO3 monomers with and without side chains.

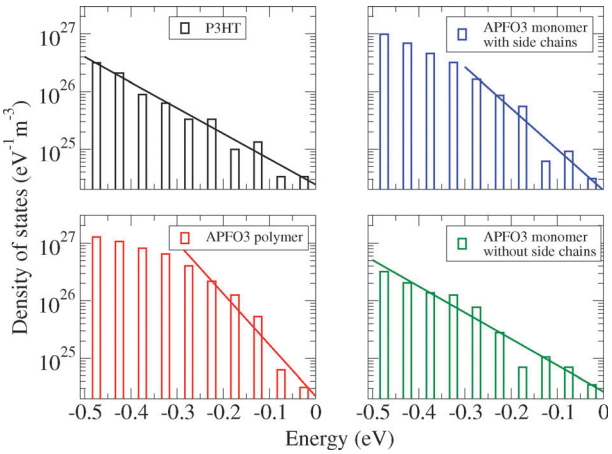

Fig. 6 The density of hole states for the systems considered in this work. Solid lines represent the fits of the tail of the density of hole states to an exponential distribution $D(E) = D_0\exp\left(-\frac{E}{E_b}\right)$, where D_0 = 2.42 × 10^{24} eV^{-1} m^{-3} and E_b = 98.0 meV for P3HT, D_0 = 2.21 × 10^{24} eV^{-1} m^{-3} and E_b = 48.9 meV for APFO3 polymer, D_0 = 1.93 × 10^{24} eV^{-1} m^{-3} and E_b = 60.9 meV for APFO3 monomer with side chains, D_0 = 2.65 × 10^{24} eV^{-1} m^{-3} and E_b = 95.1 meV for APFO3 monomer without side chains.

of well separated dipoles only if closely spaced dipoles form a nearly perfect crystal structure, which is not the case here.

3.2 Density of hole states

The difference between the diagonal disorder in various systems has been addressed so far as a way to quantify the disorder on the microscopic level. Next, it is important to understand how this disorder is reflected in the macroscopic quantities, such as the DOS and eventually the measurable properties such as the carrier mobility. The hole DOS for the systems considered in this work is presented in Fig. 6. Fits of the tail of the DOS to an exponential distribution $D(E) = D_0\exp\left(-\frac{E}{E_b}\right)$ are also presented in the figure. It was shown in ref. 30 that an exponential distribution provides an excellent fit for the tail of the DOS in P3HT. To enable the comparison of the widths of the DOS tails corresponding to different systems, the same distribution was used for fits in other systems considered in this work. As can be seen in Fig. 6, in all the cases studied, the exponential distribution provides a satisfactory, though not always an excellent fit. The parameters of the fits are given in the caption of Fig. 6.

From the values of the fitting parameters and from the general shape of the DOS graphs, one can see that generally the systems with wider distribution of onsite matrix elements (Fig. 3) exhibit a wider tail of the DOS (*i.e.* a larger E_b), in accordance with expectations. Nevertheless, there are several interesting points that are worth mentioning.

First, the DOS of P3HT has a significantly wider tail (E_b = 98.0 meV *versus* E_b = 48.9 meV) than the DOS of the APFO3 polymer, while the width of the distribution of onsite elements in P3HT (σ = 228 meV) is only somewhat wider than in the APFO3 polymer (σ = 197 meV). Therefore, there must be an additional effect that makes the DOS of P3HT significantly more disordered than in the APFO3 polymer. This effect comes from intrachain offsite electronic coupling, *i.e.* the off-diagonal disorder. Since the distribution of dihedral angles is significantly more disordered in P3HT than in the APFO3 polymer (Fig. 4, top left and bottom left), the distribution of intrachain offsite electronic coupling elements is much wider in P3HT than in the APFO3 polymer. This additionally widens the tail of the DOS in P3HT compared to the case of the APFO3 polymer. By comparing the DOS of the systems with and without interchain electronic coupling, a check was performed that the effects of interchain electronic coupling on the DOS are weak. Consequently, interchain electronic coupling does not play a role when the difference in the DOS of the studied systems is concerned. To summarize the discussion of this paragraph both the distribution of onsite and intrachain offsite matrix elements is wider in P3HT than in APFO3 and therefore the DOS tail is wider in P3HT than in APFO3.

Second, the width of the distribution of onsite matrix elements is essentially the same in the APFO3 polymer and the APFO3 monomer with side chains, while the tail of the DOS is wider in the APFO3 monomer based material (E_b = 60.9 meV *versus* E_b = 48.9 meV). The only difference between two materials comes from intrachain offsite electronic coupling present in the polymer. To understand its effect, a simple one dimensional tight-binding Hamiltonian

$$H = \sum_{i=1}^{N} \varepsilon_i \hat{a}_i^+ \hat{a}_i + \sum_{i=2}^{N} t(\hat{a}_i^+ \hat{a}_{i-1} + \hat{a}_{i-1}^+ \hat{a}_i) \qquad (2)$$

is analysed, where $\hat{a}_i$ is the annihilation operator of an electron at site i (i = 1,...,N), ε_i is the onsite energy and t is the offsite electronic coupling strength. The onsite energies are taken to have a Gaussian distribution with a standard deviation σ = 0.2 eV, while the value of t was varied to understand its role in the tail of the DOS. The DOS obtained for different values of t is presented in Fig. 7. These results demonstrate that

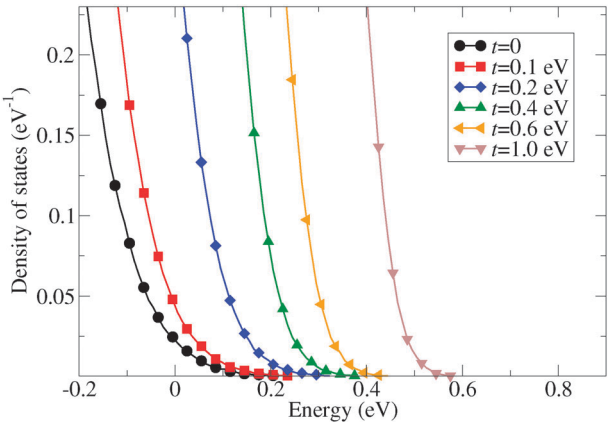

Fig. 7 The DOS for a simple one dimensional Hamiltonian with Gaussian distribution of onsite energies with σ = 0.2 eV and different values of offsite electronic coupling t.

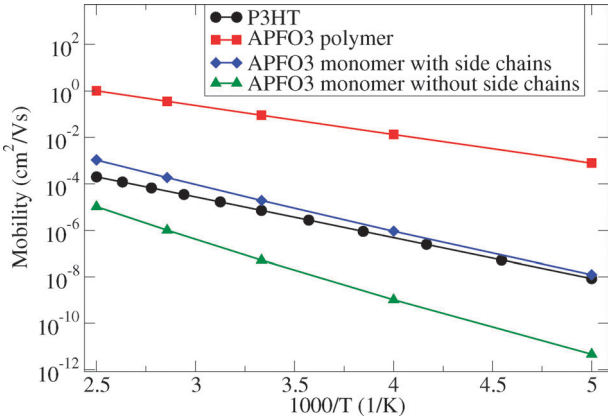

Fig. 8 Temperature dependence of mobility in the systems studied in this work. Fits of the dependence to the Arrhenius form $\mu = \mu_0 \exp\left(-\frac{E_A}{k_B T}\right)$ give the activation energies E_A = 348 meV for P3HT, E_A = 247 meV for APFO3 polymer, E_A = 392 meV for APFO3 monomer with side chains, E_A = 504 meV for APFO3 monomer without side chains.

the increase in t leads to narrowing of the tail of DOS. For this reason the intrachain offsite electronic coupling narrows the tail of the DOS in the APFO3 polymer compared to the APFO3 monomer with side chains.

It is interesting to note the different roles that intrachain offsite electronic coupling elements can have. In P3HT, they have a relatively wide distribution and therefore contribute to widening of the DOS tail. On the other hand, in APFO3 they act to narrow down the tail of the DOS. Such a pronounced difference in the role of intrachain offsite coupling elements shows the importance of their distribution for electronic properties of the material. Their narrow distribution (such as in APFO3) leads to a qualitatively different effect on the DOS tail than their wide distribution (such as in P3HT).

3.3 Hole mobility

The simulated temperature dependence of the mobility is shown in Fig. 8. In the past, we have compared the P3HT mobility results obtained using this methodology[47] with experimental data[64,65] obtained in hole only diodes in the space-charge current limited regime and the correct order of magnitude was obtained. The APFO3 material has not been studied as intensively as P3HT. Consequently, less experimental data are available for APFO3 or similar materials. In ref. 66 the room temperature field-effect transistor mobility of 1.1 × 10^{-2} cm^2 V^{-1} s^{-1} was measured for the polymer labeled PIFTBT6, which has almost the same chemical structure as APFO3. This result is in the same order of magnitude as the simulated value of 9.0 × 10^{-2} cm^2 V^{-1} s^{-1}. There are however also reports of significantly smaller values of mobility of APFO3 (10^{-4} cm^2 V^{-1} s^{-1} in ref. 67 and 68).

Activation energies obtained from the fits of the dependence to the Arrhenius form $\mu = \mu_0 \exp\left(-\frac{E_A}{k_B T}\right)$ are specified in the caption of Fig. 8. The DOS is certainly an important factor that determines the activation energy. Carriers from the tail of DOS need to be excited to energies where there are enough states so that a percolating path through the system can be formed. Nevertheless, the DOS is not the only factor – the strength of the overlaps with neighbouring states can be equally important. In line with the DOS tail widths of the P3HT and APFO3 polymers, the activation energy is smaller in APFO3 than in the P3HT polymer. On the other hand, despite the narrower DOS tail in the APFO3 monomer with side chains compared to the P3HT polymer, the P3HT polymer has a smaller activation energy. The reason for this is better wave function overlaps of neighbouring electronic states in P3HT compared to the APFO3 monomer with side chains (see Fig. S5 and S6 in ESI† which demonstrate that the distances between the neighbouring states in these materials are similar, while the overlaps are larger in P3HT). As a consequence, one needs to excite the carriers in the APFO3 monomer to larger energies before the relevant states have sufficiently good overlaps so that a percolating path can be formed.

When the comparison of mobilities of the APFO3 monomer with and without side chains is concerned, two different effects cause the differences in the mobilities. A wider tail of the DOS of the APFO3 monomer without side chains would suggest that it should have a smaller mobility. On the other hand, the presence of alkyl chains that fill the space between the monomers and act as insulating barriers for carrier transport would suggest that the APFO3 monomer with side chains should have a smaller mobility. The results presented in Fig. 8 show that the effect of the DOS prevails and consequently that the material based on the APFO3 monomer without side chains has a smaller mobility.

4 Conclusions

In conclusion, the simulations presented in this work indicate that the presence of alkyl chains reduces the diagonal disorder, while the shape of the main chains is also an important factor that affects the diagonal disorder. The tail of the DOS near the band edge tends to be wider in systems with stronger diagonal disorder. Intrachain electronic coupling has a twofold role in

the DOS tail. In relatively ordered polymers, it acts to narrow the DOS tail. In less ordered polymers, it represents an additional disorder component – the off-diagonal disorder – which acts to widen the DOS tail. Finally, the activation energy for charge carrier transport is affected not only by the width of the DOS tail, but also by typical wave function overlaps of transport states.

Acknowledgements

This work was supported by European Community FP7 Marie Curie Career Integration Grant (ELECTROMAT), Serbian Ministry of Education, Science and Technological Development (project ON171017) and FP7 projects PRACE-2IP, PRACE-3IP, HP-SEE, and EGI-InSPIRE.

References

1 H. Yan, Z. Chen, Y. Zheng, C. Newman, J. R. Quinn, F. Dtz, M. Kastler and A. Facchetti, *Nature*, 2009, **457**, 679–686.
2 J. A. Rogers, T. Someya and Y. Huang, *Science*, 2010, **327**, 1603–1607.
3 G. Giri, E. Verploegen, S. C. B. Mannsfeld, S. Atahan-Evrenk, D. H. Kim, S. Y. Lee, H. A. Becerril, A. Aspuru-Guzik, M. F. Toney and Z. Bao, *Nature*, 2011, **480**, 504–508.
4 D. L. Cheung and A. Troisi, *Phys. Chem. Chem. Phys.*, 2008, **10**, 5941–5952.
5 Y. He and Y. Li, *Phys. Chem. Chem. Phys.*, 2011, **13**, 1970–1983.
6 V. Coropceanu, J. Cornil, D. A. da Silva Filho, Y. Olivier, R. Silbey and J.-L. Bredas, *Chem. Rev.*, 2007, **107**, 926–952.
7 Z. Guo, S. A. Jenekhe and O. V. Prezhdo, *Phys. Chem. Chem. Phys.*, 2011, **13**, 7630–7636.
8 A. Dkhissi, F. Ouhib, A. Chaalane, R. C. Hiorns, C. Dagron-Lartigau, P. Iratcabal, J. Desbrieres and C. Pouchan, *Phys. Chem. Chem. Phys.*, 2012, **14**, 5613–5619.
9 Y. Li, P. Sonar, S. P. Singh, Z. E. Ooi, E. S. H. Lek and M. Q. Y. Loh, *Phys. Chem. Chem. Phys.*, 2012, **14**, 7162–7169.
10 I. D. W. Samuel and G. A. Turnbull, *Chem. Rev.*, 2007, **107**, 1272–1295.
11 Z. Shuai, L. Wang and Q. Li, *Adv. Mater.*, 2011, **23**, 1145–1153.
12 A. Salleo, T. W. Chen, A. R. Völkel, Y. Wu, P. Liu, B. S. Ong and R. A. Street, *Phys. Rev. B: Condens. Matter Mater. Phys.*, 2004, **70**, 115311.
13 R. A. Street, J. E. Northrup and A. Salleo, *Phys. Rev. B: Condens. Matter Mater. Phys.*, 2005, **71**, 165202.
14 S. D. Baranovskii, H. Cordes, F. Hensel and G. Leising, *Phys. Rev. B: Condens. Matter Mater. Phys.*, 2000, **62**, 7934–7938.
15 V. I. Arkhipov, P. Heremans, E. V. Emelianova, G. J. Adriaenssens and H. Bassler, *Appl. Phys. Lett.*, 2003, **82**, 3245–3247.
16 P. M. Borsenberger, L. Pautmeier and H. Bassler, *J. Chem. Phys.*, 1991, **94**, 5447–5454.
17 M. C. J. M. Vissenberg and M. Matters, *Phys. Rev. B: Condens. Matter Mater. Phys.*, 1998, **57**, 12964–12967.
18 J.-F. Briere and M. Cote, *J. Phys. Chem. B*, 2004, **108**, 3123–3129.
19 M. Rohlfing, M. L. Tiago and S. G. Louie, *Synth. Met.*, 2001, **116**, 101–105.
20 J. Gierschner, J. Cornil and H. J. Egelhaaf, *Adv. Mater.*, 2007, **19**, 173–191.
21 U. Salzner, J. B. Lagowski, P. G. Pickup and R. A. Poirier, *Synth. Met.*, 1998, **96**, 177–189.
22 A. Garzon, J. M. Granadino-Roldan, M. Moral, G. Garcia, M. P. Fernandez-Liencres, A. Navarro, T. Pena-Ruiz and M. Fernandez-Gomez, *J. Chem. Phys.*, 2010, **132**, 064901.
23 V. Rühle, J. Kirkpatrick and D. Andrienko, *J. Chem. Phys.*, 2010, **132**, 134103.
24 V. Rühle, A. Lukyanov, F. May, M. Schrader, T. Vehoff, J. Kirkpatrick, B. Baumeier and D. Andrienko, *J. Chem. Theory Comput.*, 2011, **7**, 3335–3345.
25 S. Kilina, E. Batista, P. Yang, S. Tretiak, A. Saxena, R. L. Martin and D. Smith, *ACS Nano*, 2008, **2**, 1381–1388.
26 P. Yang, E. R. Batista, S. Tretiak, A. Saxena, R. L. Martin and D. L. Smith, *Phys. Rev. B: Condens. Matter Mater. Phys.*, 2007, **76**, 241201.
27 D. P. McMahon and A. Troisi, *Chem. Phys. Lett.*, 2009, **480**, 210–214.
28 D. L. Cheung, D. P. McMahon and A. Troisi, *J. Am. Chem. Soc.*, 2009, **131**, 11179–11186.
29 N. Vukmirović and L.-W. Wang, *J. Phys. Chem. B*, 2009, **113**, 409–415.
30 N. Vukmirović and L.-W. Wang, *J. Phys. Chem. B*, 2011, **115**, 1792–1797.
31 X. Zhang, Z. Li and G. Lu, *Phys. Rev. B: Condens. Matter Mater. Phys.*, 2010, **82**, 205210.
32 N. Vukmirović and L.-W. Wang, *J. Chem. Phys.*, 2008, **128**, 121102.
33 N. Vukmirović and L.-W. Wang, *J. Chem. Phys.*, 2011, **134**, 094119.
34 H. Sirringhaus, P. J. Brown, R. H. Friend, M. M. Nielsen, K. Bechgaard, B. M. W. Langeveld-Voss, A. J. H. Spiering, R. A. J. Janssen, E. W. Meijer, P. Herwig and D. M. de Leeuw, *Nature*, 1999, **401**, 685–688.
35 Y. Kim, S. Cook, S. M. Tuladhar, S. A. Choulis, J. Nelson, J. R. Durrant, D. D. C. Bradley, M. Giles, I. McCulloch, C.-S. Ha and M. Ree, *Nat. Mater.*, 2006, **5**, 197–203.
36 M. Campoy-Quiles, T. Ferenczi, T. Agostinelli, P. G. Etchegoin, Y. Kim, T. D. Anthopoulos, P. N. Stavrinou, D. D. C. Bradley and J. Nelson, *Nat. Mater.*, 2008, **7**, 158–164.
37 R. B. Ross, C. M. Cardona, D. M. Guldi, S. G. Sankaranarayanan, M. O. Reese, N. Kopidakis, J. Peet, B. Walker, G. C. Bazan, E. Van Keuren, B. C. Holloway and M. Drees, *Nat. Mater.*, 2008, **8**, 208–212.
38 A. Tada, Y. F. Geng, Q. S. Wei, K. Hashimoto and K. Tajima, *Nat. Mater.*, 2011, **10**, 450–455.
39 C. Kitamura, S. Tanaka and Y. Yamashita, *Chem. Mater.*, 1996, **8**, 570–578.
40 O. Inganäs, F. Zhang and M. R. Andersson, *Acc. Chem. Res.*, 2009, **42**, 1731–1739.
41 O. Inganäs, M. Svensson, F. Zhang, A. Gadisa, N. K. Persson, X. Wang and M. R. Andersson, *Appl. Phys. A: Mater. Sci. Process.*, 2004, **79**, 31–35.

42 S. K. Pal, T. Kesti, M. Maiti, F. Zhang, O. Inganäs, S. Hellström, M. R. Andersson, F. Oswald, F. Langa, T. Österman, T. Pascher, A. Yartsev and V. Sundström, *J. Am. Chem. Soc.*, 2010, **132**, 12440–12451.

43 C. S. Ponseca, A. Yartsev, E. Wang, M. R. Andersson, D. Vithanage and V. Sundström, *J. Am. Chem. Soc.*, 2012, **134**, 11836–11839.

44 H. Némec, P. Kužel and V. Sundström, *J. Photochem. Photobiol., A*, 2010, **215**, 123–139.

45 H. Némec, H.-K. Nienhuys, F. Zhang, O. Inganäs, A. Yartsev and V. Sundström, *J. Phys. Chem. C*, 2008, **112**, 6558–6563.

46 C. S. Ponseca, H. Némec, N. Vukmirović, S. Fusco, E. Wang, M. R. Andersson, P. Chabera, A. Yartsev and V. Sundström, *J. Phys. Chem. Lett.*, 2012, **3**, 2442–2446.

47 N. Vukmirović and L.-W. Wang, *Nano Lett.*, 2009, **9**, 3996–4000.

48 N. Vukmirović and L.-W. Wang, *Phys. Rev. B: Condens. Matter Mater. Phys.*, 2010, **81**, 035210.

49 A. S. Anselmo, L. Lindgren, J. Rysz, A. Bernasik, A. Budkowski, M. R. Andersson, K. Svensson, J. van Stam and E. Moons, *Chem. Mater.*, 2011, **23**, 2295–2302.

50 J. Mardalen, E. J. Samuelsen, O. R. Gautun and P. H. Carlsen, *Solid State Commun.*, 1991, **77**, 337–339.

51 J. Mardalen, E. J. Samuelsen, O. R. Gautun and P. H. Carlsen, *Synth. Met.*, 1992, **48**, 363–380.

52 S. Marchant and P. J. S. Foot, *Polymer*, 1997, **38**, 1749–1751.

53 S.-S. Kim, S.-I. Na, J. Jo, G. Tae and D.-Y. Kim, *Adv. Mater.*, 2007, **19**, 4410–4415.

54 J. R. Maple, M.-J. Hwang, T. P. Stockfisch, U. Dinur, M. Waldman, C. S. Ewig and A. T. Hagler, *J. Comput. Chem.*, 1994, **15**, 162–182.

55 M. J. Hwang, T. P. Stockfisch and A. T. Hagler, *J. Am. Chem. Soc.*, 1994, **116**, 2515–2525.

56 L.-W. Wang, *Phys. Rev. B: Condens. Matter Mater. Phys.*, 2002, **65**, 153410.

57 L.-W. Wang, *Phys. Rev. Lett.*, 2002, **88**, 256402.

58 L.-W. Wang, *Appl. Phys. Lett.*, 2001, **78**, 1565–1567.

59 J. Li and L.-W. Wang, *Phys. Rev. B: Condens. Matter Mater. Phys.*, 2005, **72**, 125325.

60 K. D. Meisel, H. Vocks and P. A. Bobbert, *Phys. Rev. B: Condens. Matter Mater. Phys.*, 2005, **71**, 205206.

61 S. S. Zade and M. Bendikov, *Chemistry*, 2008, **14**, 6734–6741.

62 R. Coehoorn, W. F. Pasveer, P. A. Bobbert and M. A. J. Michels, *Phys. Rev. B: Condens. Matter Mater. Phys.*, 2005, **72**, 155206.

63 N. Vukmirović and L.-W. Wang, *Appl. Phys. Lett.*, 2010, **97**, 043305.

64 C. Tanase, E. J. Meijer, P. W. M. Blom and D. M. de Leeuw, *Phys. Rev. Lett.*, 2003, **91**, 216601.

65 N. I. Craciun, J. Wildeman and P. W. M. Blom, *Phys. Rev. Lett.*, 2008, **100**, 056601.

66 Q. Zheng, B. J. Jung, J. Sun and H. E. Katz, *J. Am. Chem. Soc.*, 2010, **132**, 5394–5404.

67 W. Li, R. Qin, Y. Zhou, M. Andersson, F. Li, C. Zhang, B. Li, Z. Liu, Z. Bo and F. Zhang, *Polymer*, 2010, **51**, 3031–3038.

68 L. M. Andersson, *Org. Electron.*, 2011, **12**, 300–305.